Supplementary Information for:

Diagnosing spatial biases and uncertainties in global fire emissions inventories: Indonesia as regional case study

T. Liu, L. J. Mickley, M. E. Marlier, R. S. DeFries, M. F. Khan, M. T. Latif, and A. Karambelas

S1. Inventory-specific relative fire confidence scores

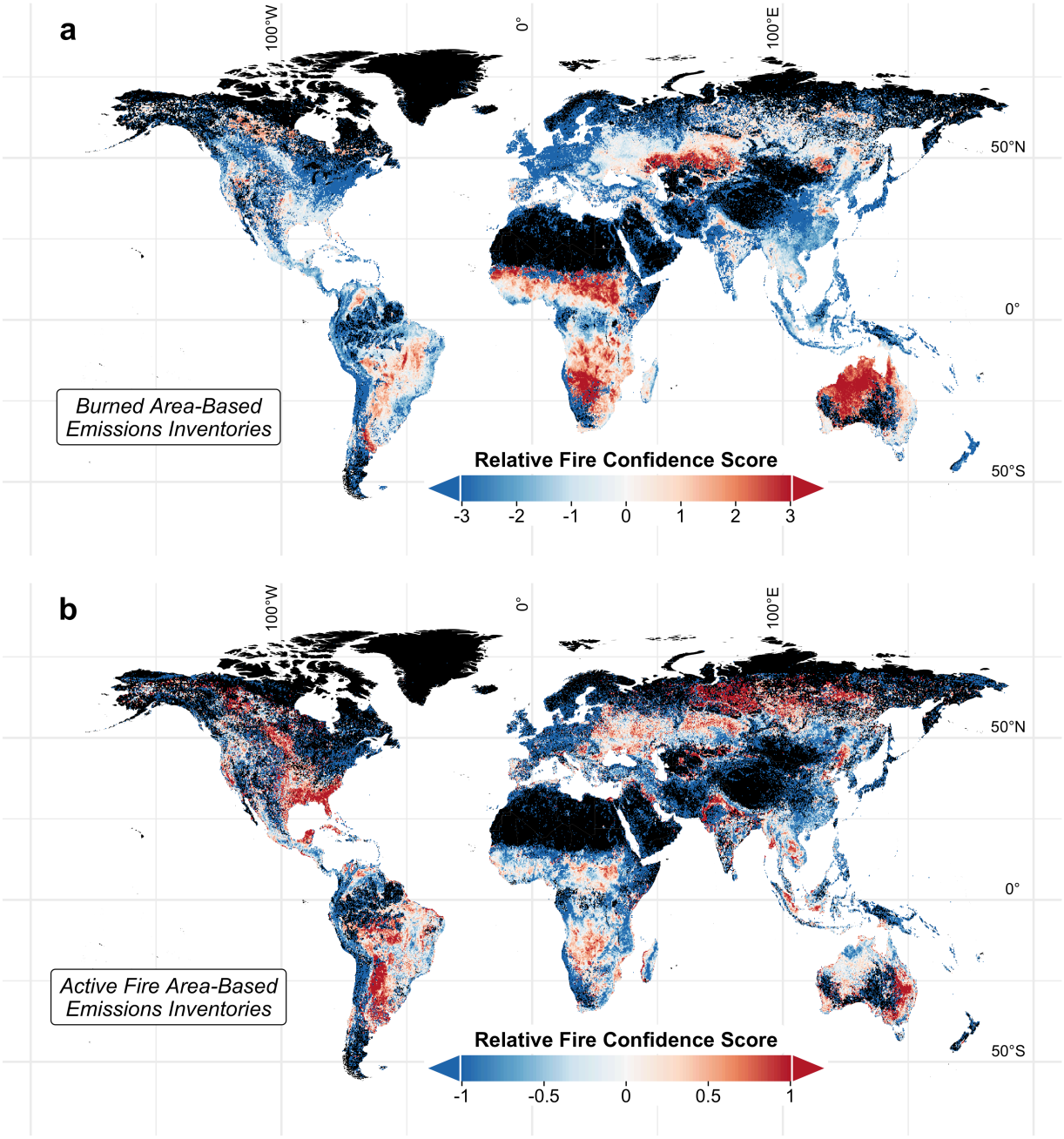

Figure S1. Relative fire confidence score for bottom-up emissions inventories based primarily on (**a**) MODIS MCD64A1 burned area (BA-score; e.g. GFEDv4s) and (**b**) MODIS MxD14A1 active fire pixel area (AFA-score; e.g. FINN). The darkest blue pixels represent grid cells with (**a**) active fire observations but no burned area over 2003-2017 or (**b**) burned area but no active fire observations over this time frame. Thus, these grid cells indicate low confidence for (**a**) burned area inventories or (**b**) active fire pixel inventories.

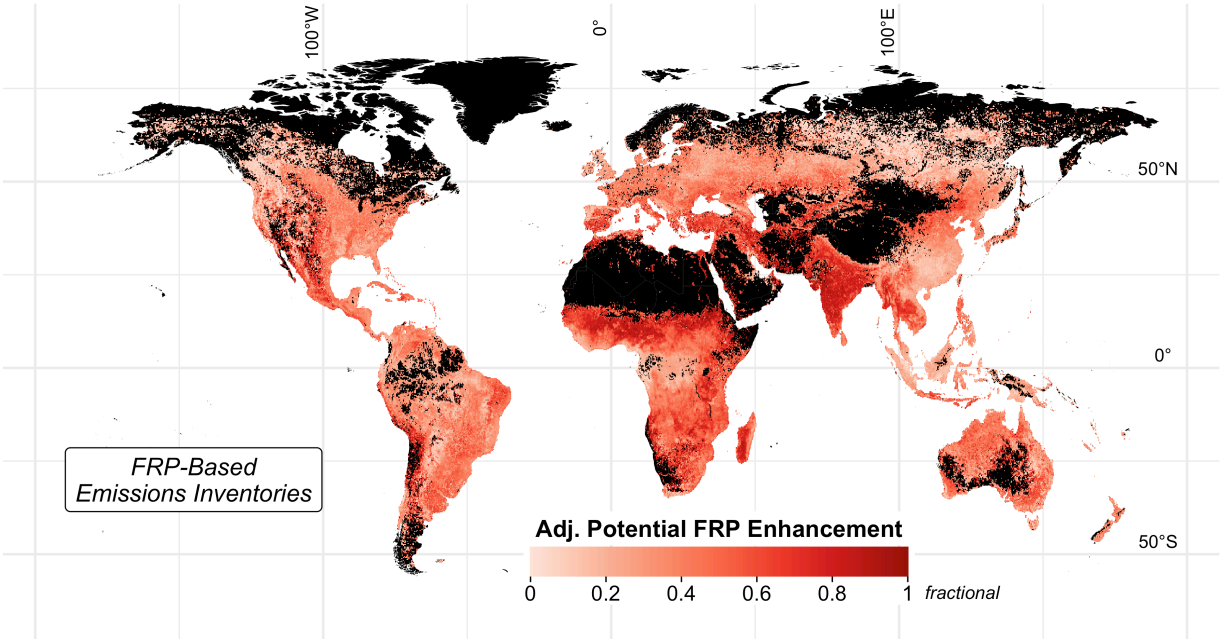

Figure S2. Adjusted potential FRP enhancement (pFRP), expressed as fractional fire energy, for top-down FRP-based emissions inventories. The potential FRP enhancement diagnoses additional fire energy, unaccounted for by the MODIS active fires product but indicated by large burn scars from the MODIS burned area product or very small fires from the 375-m VIIRS active fires product. It is the sum of fractional MODIS/Terra + Aqua MxD14A1 FRP outside MCD64A1 burned area and fractional VIIRS FRP outside the MODIS burn extent, then adjusted by the FRP-weighted cloud/haze obscuration fraction. High pFRP is associated with lower confidence, as many MODIS active fire observations are not co-located with MODIS burned area or VIIRS FRP observations.

S2. Global fire emissions inventories: "bottom-up" and "top-down" methods

S2.1 Bottom-up emissions inventories: GFED and FINN

Bottom-up emission inventories (e.g. GFED and FINN) multiply burned area, fuel load, combustion completeness, and emissions factors to estimate fire emissions:

$$E_i = BA\ x\ f_b\ x\ \gamma\ x\ EF_i \quad \text{(S1)}$$

where E_i is emissions of species i, BA is burned area, f_b is the fraction of biomass burned or fuel load, γ is combustion completeness, and EF_i is the emissions factor of species i (van der Werf et al., 2017; Wiedinmyer et al., 2011). GFEDv4s relies on 500-m burned area observations with a "small fires boost" (SFB) from active fire geolocations to estimate monthly emissions (van der Werf et al., 2017). FINN uses daily 1-km active fire area as "burned area" (Wiedinmyer et al., 2011).

GFEDv4s is available at 0.25° x 0.25° spatial resolution and monthly timesteps with daily fraction based on active fire counts and burned area (Mu et al., 2011). This inventory uses active fire detections from Tropical Rainfall Measuring Mission (TRMM) Visible and Infrared Scanner (VIRS) and Along Track Scanning Radiometer (ASTR) to estimate monthly emissions for the pre-MODIS era (from 1997-2000). GFEDv4s also projects fire emissions (2017-2018) based on the observed relationships between historical GFEDv4s emissions and MODIS active fires. For the small fires boost, GFEDv4s uses MCD14ML C6 active fire geolocations (Randerson et al., 2012), but for burned area, the inventory currently relies on MCD64A1 C5.1, rather than C6 (Giglio et al., 2013). GFED uses the Carnegie Ames Stanford Approach (CASA) biogeochemical model to estimate fire carbon and dry matter (DM) emissions using burned area, meteorology, net primary production, and land cover as input variables (van der Werf et al., 2010).

FINNv1.5 is available at the native MODIS 1-km spatial resolution from 2002 and available at near real time. FINNv1.5 derives active fire area from MCD14DL C5 (C6 from 2017-present) active fire geolocations, which is the near-real-time equivalent of MCD14ML. FINN assumes an upper-bound estimate of burned area (1 km^2) for each fire detection for most fires except for grassland or savanna fires, which are assigned a burned area of 0.75 km^2 (Wiedinmyer et al., 2011). FINN assigns fuel loadings by region and land cover, based on Hoelzemann et al. (2004). A newer version of this inventory, FINNv1.6 is no longer available as of April 2018 due to dataset issues and has been reverted back to FINNv1.5 (http://bai.acom.ucar.edu/Data/fire/).

For land cover, GFEDv4s and FINNv1.5 use the 500-m MCD12Q1 C5.1 land cover product. Neither GFEDv4s nor FINNv1.5 has updated the respective LULC maps from C5.1 to C6. GFEDv4s separately incorporates peat maps (Olson et al., 2001) and emissions factors (Christian et al., 2003). FINNv1.5 subdivides the broader savanna, grassland, and shrubland class into savanna/grassland and woody savanna/shrubland subclasses and further delineates a temperate evergreen forest subclass from the broader temperate forest class.

S2.2 Top-down emissions inventories: GFAS, QFED, and FEER

Top-down emissions inventories (e.g. GFAS, QFED, and FEER) integrate daily FRP to fire radiative energy (FRE) and scale this quantity linearly to obtain fire emissions:

$$FRE = \int_{t_1}^{t_2} FRP(t)dt \quad \text{(S2)}$$

$$E_i = FRE \; x \; \beta \; x \; EF_i \quad \text{(8)} \quad \text{OR} \quad E = FRE \; x \; C_e \quad \text{(S3)}$$

where FRE is the integral of FRP from time t_1 to t_2, β is a coefficient converting FRP to dry matter, and C_e is the coefficient of emissions that is equivalent to the product of β and EF_i for total particulate matter (TPM) in Eq. S2 (Darmenov and da Silva, 2013; Ichoku and Ellison, 2014; Kaiser et al., 2012). Eq. S2 applies to GFAS and QFED, while Eq. S3 applies to FEER. In some inventories, such as GFAS, the coefficient β varies with class of LULC. The FRP-based inventories also statistically adjust FRP for spatial and temporal gaps in the observations due to cloud cover (Kaiser et al., 2012), but by assuming that fire persists through cloudy days, such adjustments may result in unrealistic emissions (Di Giuseppe et al., 2017). GFAS and QFED directly use MxD14 FRP, while FEER relies on the GFAS FRP after adjustment for cloud gaps.

To convert FRP to DM burned, GFASv1.2 uses conversion factors derived from GFEDv3 DM combustion rates (Kaiser et al., 2012). QFED globally calibrates emissions coefficients with GFEDv2 but further boosts the emissions of aerosols (OC, BC, $PM_{2.5}$). Based on constraints from observed smoke AOD, QFED applies global emission strength factors that range from 1.8-4.5, depending on land cover (Darmenov and da Silva, 2013). Similarly, Kaiser et al. (2012) recommended a global scaling factor of 3.4 for GFAS OC and BC emissions to reconcile with smoke AOD observations. FEER estimates TPM emissions by directly applying smoke AOD-derived emissions coefficients to FRP observations by region and land cover, and then converts TPM to other species using emissions factors (Ichoku and Ellison, 2014).

QFEDv2.5r1, GFASv1.2, and FEERv1.0-G1.2 are available on a daily basis at near real time and 0.1° x 0.1° spatial resolution. GFASv1.2 switched from using C5 to C6 MxD14 FRP after December 2016, but has not retroactively updated emissions from before that; this discrepancy may lead to inconsistencies in the timeseries of GFASv1.2 emissions (Giglio et al., 2016). FEERv1.0-G1.2 relies on GFASv1.2 FRP as input. QFEDv2.5r1 uses the MxD14 C6 FRP. For land cover, GFASv1.2 currently considers only the LULC with the highest emissions in each 0.5° x 0.5° grid cell, which it derives from GFED3. Like GFEDv4s, GFASv1.2 separately delineates peatland emissions (Heil et al., 2010). FEER uses a dominant fire-prone LULC map, derived from MODIS, at 1° x 1° spatial resolution. QFEDv2.5r1 uses the simplest LULC classification, without either peatland or agricultural classes; in addition, while QFED separates the grassland and savanna classes, they are treated as the same LULC both in terms of emissions factors and aerosol emissions enhancements.

Table S1. Emissions factors (g species kg^{-1} dry matter) for CO_2, CO, CH_4, organic carbon (OC), black carbon (BC) and fine particulate matter ($PM_{2.5}$) used in the global fire emissions inventories

Inventory	Species	Land Use and Land Cover (LULC)					
		SAVA *Savanna, Grassland, Shrubland*	**BORF** *Boreal Forest*	**TEMF** *Temperate Forest*	**DEFO** *Tropical Forest*	**PEAT** *Peatland*	**AGRI** *Agricultural*
GFEDv4s	CO_2	1686	1489	1647	1643	1703	1585
FINNv1.0		1716/1692[a]	1514	1630	1643	—	1537
GFASv1.0		1646	1572[b]		1626	1703	1308
QFEDv2.4		1613	1569[b]		1580	—	—
GFEDv4s	CO	63	127	88	93	210	102
FINNv1.0		68/59[a]	118	102	92	—	111
GFASv1.0		61	106[b]		101	210	92
QFEDv2.4		65	107[b]		104	—	—
GFEDv4s	CH_4	1.94	5.96	3.36	5.07	20.8	5.82
FINNv1.0		2.6/1.5[a]	6	5	5.1	—	6
GFASv1.0		2.2	4.8[b]		6.6	20.8	8.4
QFEDv2.4		2.3	4.7[b]		6.8	—	—
GFEDv4s	OC	2.62	9.6	9.6	4.71	6.02	2.3
FINNv1.0		6.6/2.6[a]	7.8	9.2	4.7	—	3.3
GFASv1.0		3.2	9.1[b]		4.3	6.0	4.2
QFEDv2.4		3.4	8.6-9.7[b]		5.2	—	—
GFEDv4s	BC	0.37	0.5	0.5	0.52	0.04	0.75
FINNv1.0		0.5/0.37[a]	0.2	0.56	0.52	—	0.69
GFASv1.0		0.46	0.56[b]		0.57	0.04	0.42
QFEDv2.4		0.48	0.56[b]		0.66	—	—
GFEDv4s	$PM_{2.5}$	7.17	15.3	12.9	9.1	9.1	6.26
FINNv1.0		15.4/8.3[a]	13	13	9.7	—	5.8
GFASv1.0		4.9	13.8[b]		9.1	9.1	8.3
QFEDv2.4		5.4	13[b]		9.1	—	—

[a] Woody savanna/shrubland and savanna/grassland. [b] Extratropical forest (BORF and TEMF).
[c] Peatland and agricultural regions are treated as tropical forest, temperate forest, boreal forest, or savanna/grassland if specific emission factor is not indicated.

S3. Validation of smoke exposure in Equatorial Asia from Indonesia fires

S3.1 Singapore

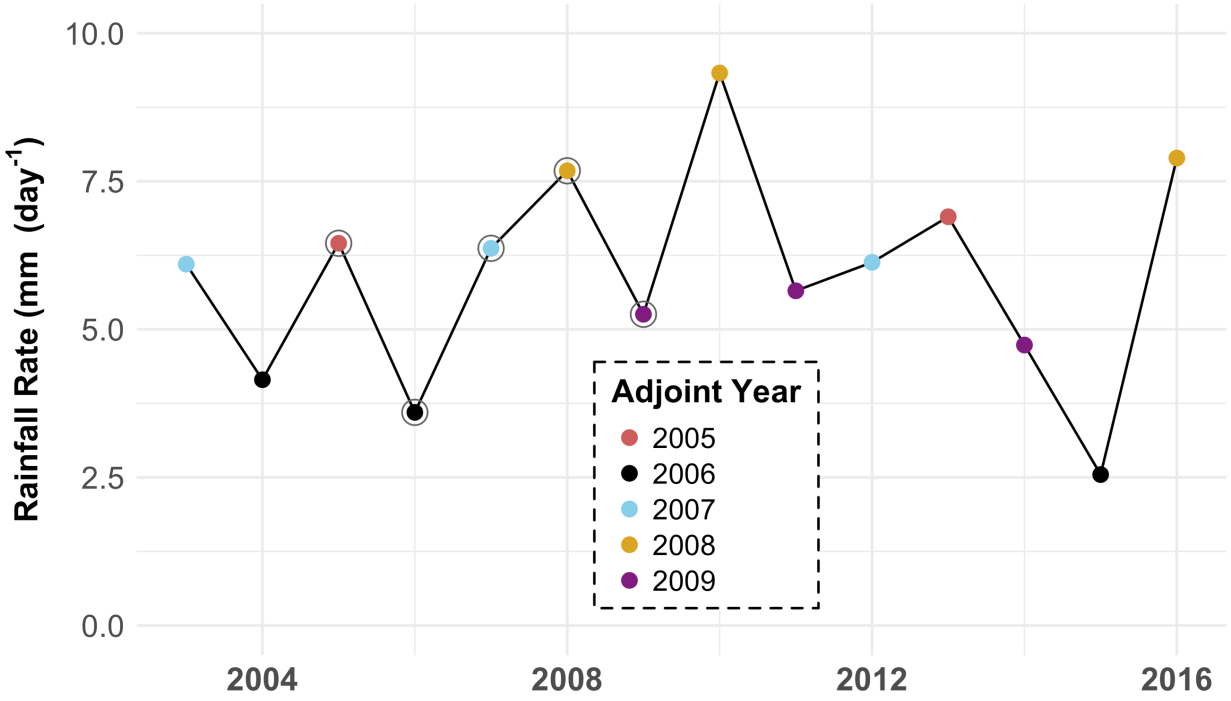

Figure S3. Average CHIRPS rainfall rate (mm day^{-1}) over Sumatra and Kalimantan, from 2003-2016. The years 2003-2004 and 2010-2016 are colored according to their closest match in the average rainfall rate during years with adjoint sensitivities (2005-2009), which are also colored but circled with dark gray outlines.

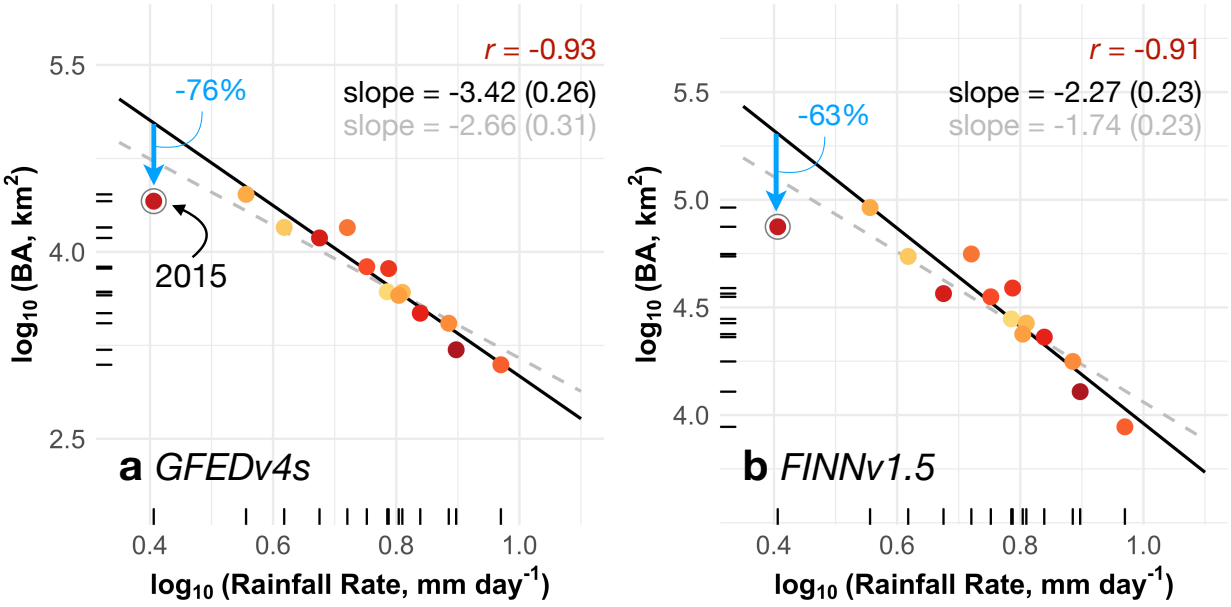

Figure S4. Under-detection of 2015 Indonesia fires in burned area relative to the 2003-2016 period (similar to Figure 9). CHIRPS rainfall rates (mm day^{-1}) are plotted against MODIS (**a**) GFEDv4s burned area and (**b**) FINNv1.5 active fire area in log-log space. All variables are averaged temporally over July-October and spatially over Sumatra and Kalimantan, Indonesia. Colors denote different years from 2003-2016, with later years depicted by redder shades; values for 2015 are circled. Inset shows the correlation (r, $p < 0.01$), slope of the linear regression (gray dashed line), and slope with 2015 removed (black line) for each pair of observations. Standard errors for the slopes are shown in parentheses. There is no statistically significant linear trend in any variable. Blue arrows show that observed burned area is lower than expected based on prediction from the linear regression of rainfall and fires that excludes 2015 observations. Percent underestimate of each fire variable based on these predictions is shown in blue.

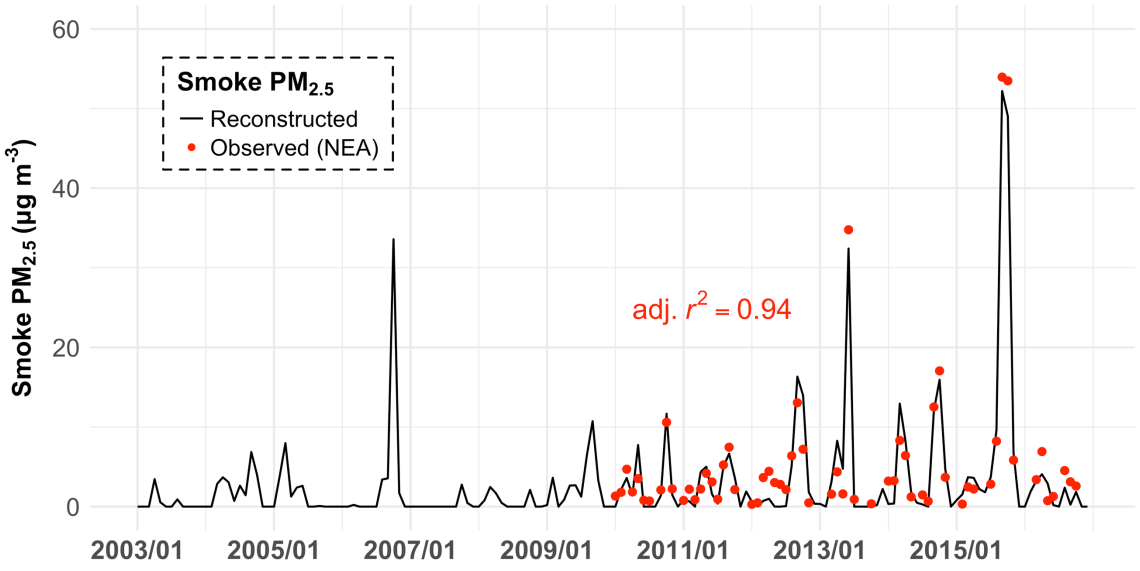

Figure S5. Observed (red) and reconstructed (black) smoke $PM_{2.}$ in Singapore for 2003-2016. Observations are from the Singapore NEA. We reconstruct $PM_{2.5}$ over 2003 to 2009 by building a model based on the observed 2010-2016 $PM_{2.5}$ record and four meteorological variables (visibility, air temperature, wind speed, and rainfall) observed at the Singapore Changi Airport. Adjusted r^2 for the model versus observations over 2010-2016 is 0.94. A baseline $PM_{2.5}$ of 13.77 µg m^{-3}, calculated as the median of $PM_{2.5}$ during non-fire season months (January to June, November to December), is subtracted from observations to obtain smoke $PM_{2.5}$.

S3.2 Malaysia and Indonesia

Malaysia. We use PM_{10} observations across a network of 59 residential and industrial Continuous Air Quality Monitoring (CAQM) stations in Malaysia, maintained by the Malaysian Department of Environment since 1996, to further validate our modeled population-weighted smoke exposure (Khan et al., 2015; Kuwata et al., 2018; Figure S6). Two stations, CAE 022 and CAK 029, do not have observations from 2003-2015, so we exclude these stations in our analysis (Table S2). To weight these observations by population, we use the population density estimates from the Gridded Population of the World, version 4.1, adjusted to the country totals from the United Nations' *World Population Prospects* country totals (UN WPP-adjusted GPWv4.1), at the native 1 km x 1 km spatial resolution (CIESIN, 2017). We first interpolate the 5-yearly population density linearly to annual values and extract the population density in the grid cell co-located with each station. We subtract the background PM_{10}, here defined as median PM_{10} during non-fire season months, from monthly mean PM_{10} observations at each station, and then take the population-weighted average across all stations, yielding the monthly smoke PM_{10} for the 2003-2015 time period.

Indonesia. Due to the lack of ground observations of $PM_{2.5}$ and PM_{10} in Indonesia, we use monthly satellite-derived AOD, from MODIS/Terra and Aqua MOD/MYD08_M3, from 2003-2016, for validation of Indonesia population-weighted exposure. We use the MxD08_M3 C6 aerosol optical thickness (AOT) at 0.55 µm, available at 1° x 1° spatial resolution and in the

GEE data catalog. We subtract monthly AOD, averaged over Indonesia, by mean AOD of non-fire season months to estimate smoke AOD.

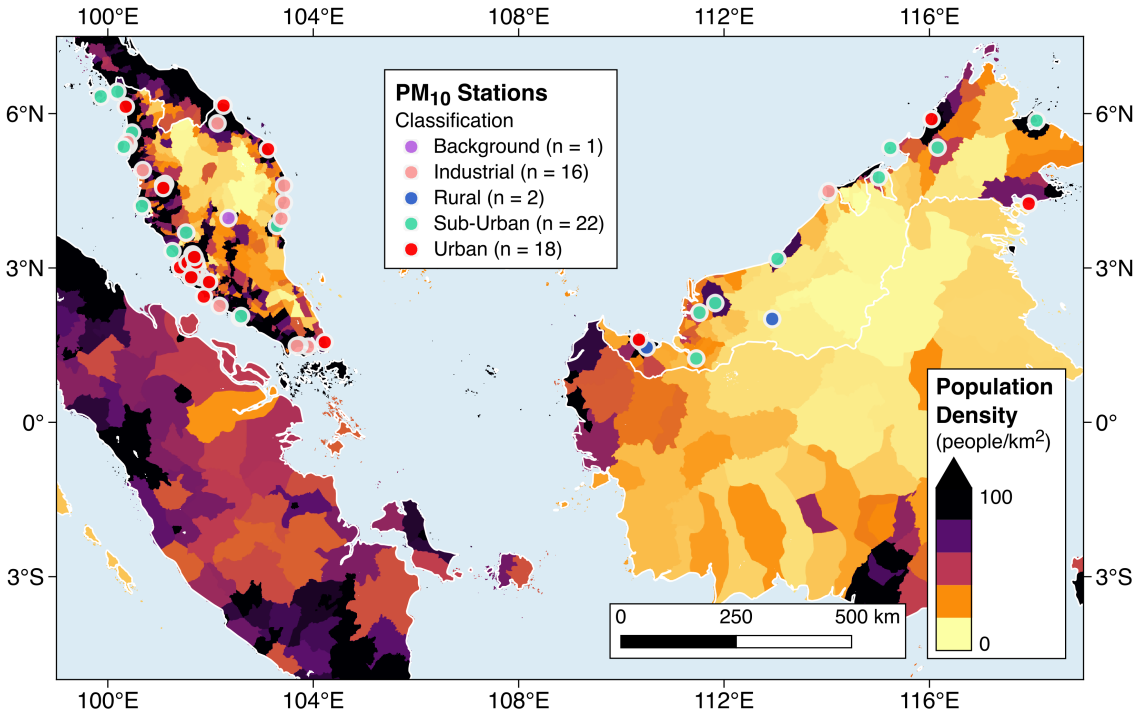

Figure S6. PM_{10} station network (n = 59) in Malaysia overlaid on population density in 2010. The different colors of the station sites denote different environments, classified according to the locations of the stations (background, industrial, rural, sub-urban, or urban).

Table S2. Details on PM_{10} stations in Malaysia used for validation of modeled population-weighted exposure.

Station ID	Location		Time Period	Pop. Density (people/km^2)	Classification
	Coordinates	State			
CAS 001	103.9°E, 1.5°N	Johor	2003-2015	1975	Industrial
CAE 002	103.4°E, 4.3°N	Terengganu	2003-2015	334	Industrial
CAN 003	100.4°E, 5.4°N	Pulau Pinang	2003-2015	2447	Industrial
CAK 004	110.4°E, 1.6°N	Sarawak	2003-2015	451	Industrial
CAC 005	101.7°E, 3.3°N	Selangor	2003-2008	2271	Sub-Urban
CAS 006	102.2°E, 2.3°N	Melaka	2003-2015	1161	Industrial
CAE 007	102.3°E, 4°N	Pahang	2003-2015	97	Background
CAN 008	101.1°E, 4.6°N	Perak	2003-2015	906	Industrial
CAN 009	100.4°E, 5.4°N	Pulau Pinang	2003-2015	2437	Sub-Urban
CAC 010	101.8°E, 2.8°N	Negeri Sembilan	2003-2015	466	Industrial
CAC 011	101.4°E, 3°N	Selangor	2003-2015	1451	Urban
CAC 012	101.7°E, 3.1°N	Kuala Lumpur	2003-2004	5334	Urban
CAN 013*	101.1°E, 4.6°N	Perak	1997-1999	906	Sub-Urban
CAE 014	103.3°E, 3.8°N	Pahang	2003-2015	426	Sub-Urban
CAE 015	103.4°E, 4°N	Pahang	2003-2015	203	Industrial
CAC 016	101.6°E, 3.1°N	Selangor	2003-2015	3875	Industrial
CAN 017	100.5°E, 5.6°N	Kedah	2003-2015	2135	Sub-Urban
CAN 018*	100.4°E, 5.4°N	Pulau Pinang	1996-1998	4205	Industrial
CAS 019	103.7°E, 1.5°N	Johor	2003-2015	3502	Industrial
CAN 020	100.7°E, 4.9°N	Perak	2003-2015	1597	Industrial
CAE 022	102.3°E, 6.2°N	Kelantan	2003-2015	1326	Urban
CAC 023	101.7°E, 3°N	Selangor	2003-2010	2726	Sub-Urban
CAE 024	103.4°E, 4.6°N	Terengganu	2003-2015	215	Industrial
CAC 025	101.6°E, 3.1°N	Selangor	2003-2015	3762	Urban
CAK 026	111.8°E, 2.3°N	Sarawak	2003-2015	79	Sub-Urban
CAK 027	113°E, 3.2°N	Sarawak	2003-2015	80	Sub-Urban
CAK 028	114°E, 4.4°N	Sarawak	2003-2015	489	Sub-Urban
CAK 029	111.5°E, 2.1°N	Sarawak	2003-2015	48	Sub-Urban
CAH 030	116°E, 5.9°N	Sabah	2003-2015	1493	Urban
CAK 031	115°E, 4.8°N	Sarawak	2003-2015	51	Sub-Urban
CAN 032	99.9°E, 6.3°N	Kedah	2003-2015	211	Sub-Urban

CAN 033	100.2°E, 6.4°N	Perlis	2003-2015	740	Sub-Urban
CAE 034	103.1°E, 5.3°N	Terengganu	2003-2015	3068	Urban
CAK 035	110.5°E, 1.5°N	Sarawak	2003-2015	205	Rural
CAK 036	111.5°E, 1.2°N	Sarawak	2003-2015	25	Sub-Urban
CAN 038	100.3°E, 5.4°N	Pulau Pinang	2003-2015	6313	Sub-Urban
CAH 039	117.9°E, 4.2°N	Sabah	2003-2015	67	Urban
CAN 040	100.3°E, 6.1°N	Kedah	2003-2015	2205	Urban
CAN 041	100.7°E, 4.2°N	Perak	2003-2015	257	Sub-Urban
CAH 042	115.2°E, 5.3°N	Labuan	2003-2015	919	Sub-Urban
CAS 043	102.6°E, 2°N	Melaka	2003-2015	2274	Urban
CAS 044	102.6°E, 2.1°N	Johor	2003-2015	2274	Sub-Urban
CAC 045	101.5°E, 3.7°N	Perak	2003-2015	103	Sub-Urban
CAN 046	101.1°E, 4.6°N	Perak	2003-2015	906	Urban
CAC 047	102°E, 2.7°N	Negeri Sembilan	2003-2015	1899	Urban
CAC 048	101.3°E, 3.3°N	Selangor	2003-2015	460	Sub-Urban
CAH 049	116.2°E, 5.3°N	Sabah	2003-2015	48	Sub-Urban
CAH 050	118.1°E, 5.9°N	Sabah	2003-2015	172	Sub-Urban
CAS 051	103.7°E, 1.5°N	Johor	2003-2008	1745	Industrial
CAK 052	110.3°E, 1.6°N	Sarawak	2003-2007	451	Urban
CAC 053	101.7°E, 2.9°N	W. P. Putrajaya	2003-2015	1392	Urban
CAC 054	101.7°E, 3.1°N	Kuala Lumpur	2004-2015	5774	Urban
CAK 055	112.9°E, 2°N	Sarawak	2004-2015	4	Rural
CAC 056	101.9°E, 2.4°N	Negeri Sembilan	2007-2015	162	Urban
CAS 057	104.2°E, 1.6°N	Johor	2008-2015	83	Urban
CAC 058	101.7°E, 3.2°N	Kuala Lumpur	2009-2015	6243	Urban
CAE 059	102.1°E, 5.8°N	Kelantan	2009-2015	393	Industrial
CAC 060	101.6°E, 2.8°N	Selangor	2010-2015	299	Urban
CAK 061	114°E, 4.5°N	Sarawak	2010-2015	489	Industrial

* Stations CAN 013 and CAN 018 do not have any observations during the 2003-2015 study period, and so are not included in our analysis.

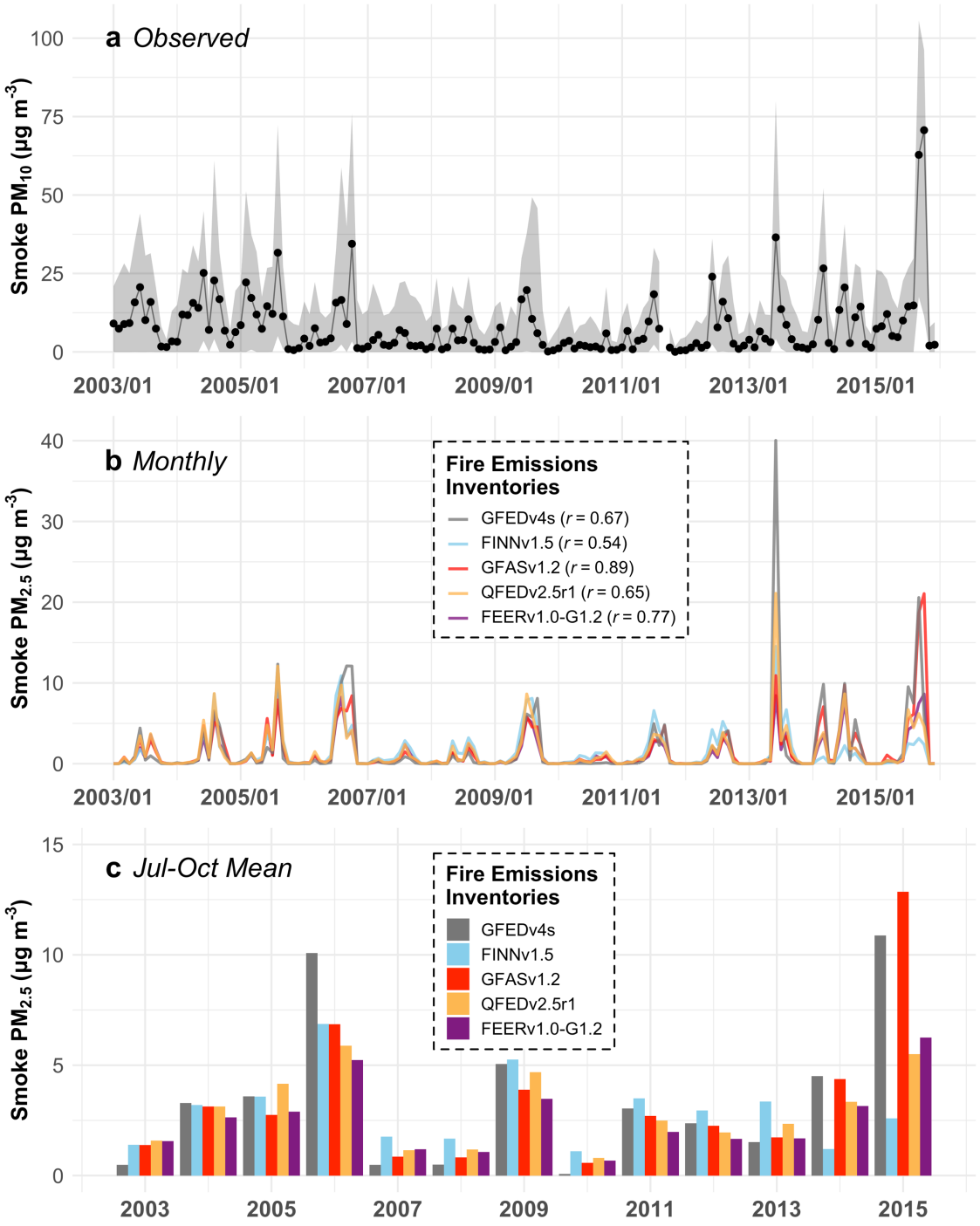

Figure S7. Smoke $PM_{2.5}$ exposure in Malaysia, from 2003-2015. (**a**) Observed, population-weighted observed smoke PM_{10} from 2003-2015, using 57 stations (Table S2), with the gray envelope showing the 5th-95th quantile range. (**b**) Modeled, population-weighted smoke $PM_{2.5}$ calculated by the GEOS-Chem adjoint with different global fire emissions inventories: GFEDv4s, FINNv1.5, GFASv1.2, QFEDv2.5r1, and FEERv1.0-G1.2. Correlations between observed smoke PM_{10} and modeled smoke $PM_{2.5}$ are shown inset for each inventory. All correlations are statistically significant ($p < 0.01$). (**c**) Jul-Oct mean smoke $PM_{2.5}$ by inventory.

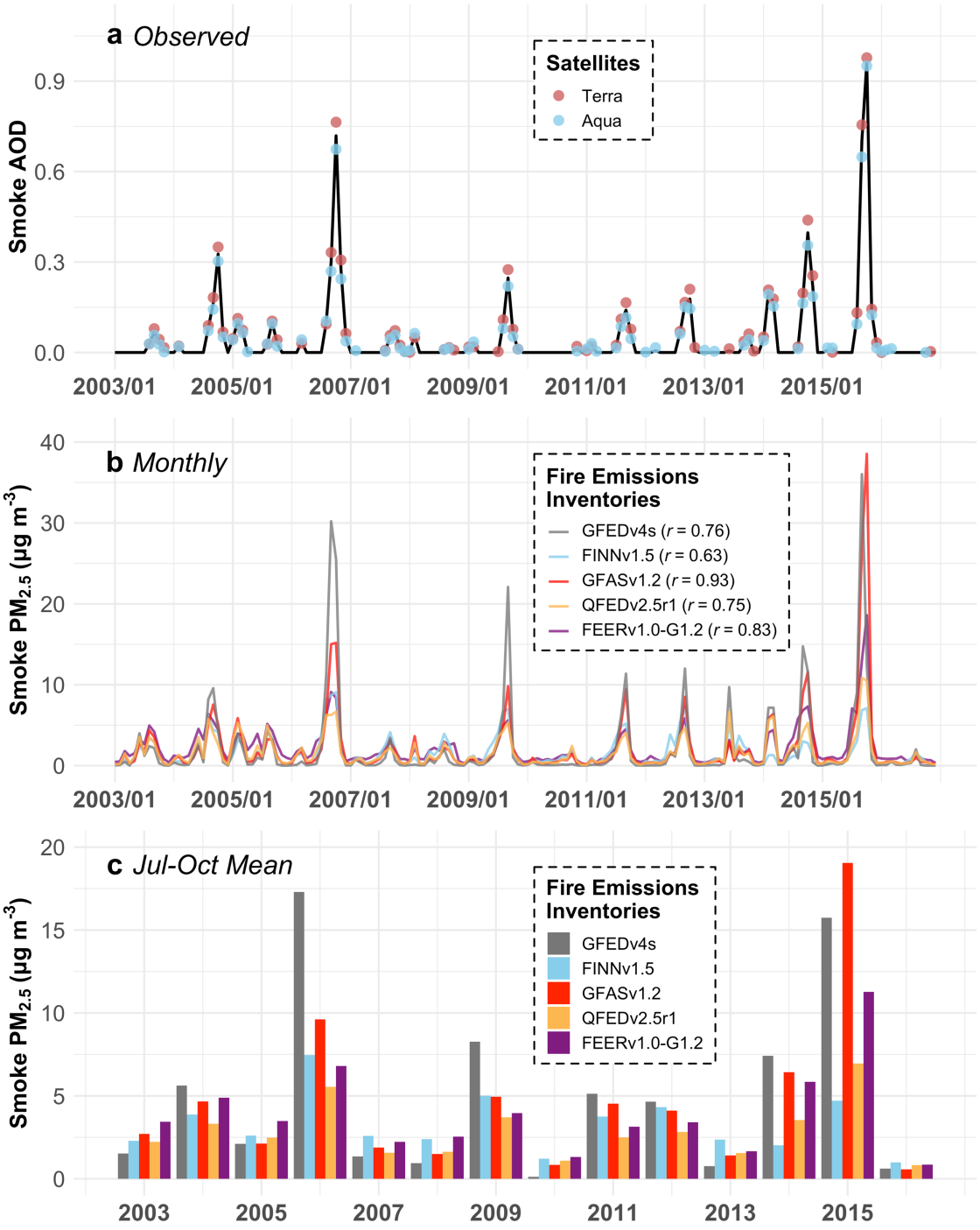

Figure S8. Smoke AOD and $PM_{2.5}$ exposure in Indonesia, from 2003-2016. (**a**) Smoke aerosol optical depth (AOD) from 2003-2016, derived from the average of MODIS Terra (red circles) and Aqua (blue circles) smoke AOD over Indonesia (Sumatra and Kalimantan). (**b**) Modeled, population-weighted smoke $PM_{2.5}$ calculated by the GEOS-Chem adjoint for this region, using different global fire emissions inventories: GFEDv4s, FINNv1.5, GFASv1.2, QFEDv2.5r1, and FEERv1.0-G1.2. Correlations between observed smoke AOD and modeled smoke $PM_{2.5}$ are shown inset for each inventory. All correlations are statistically significant ($p < 0.01$). (**c**) Jul-Oct mean smoke $PM_{2.5}$ by inventory.

S4. Ancillary information on burn date uncertainty, fire diurnal cycle, and land use/ land cover

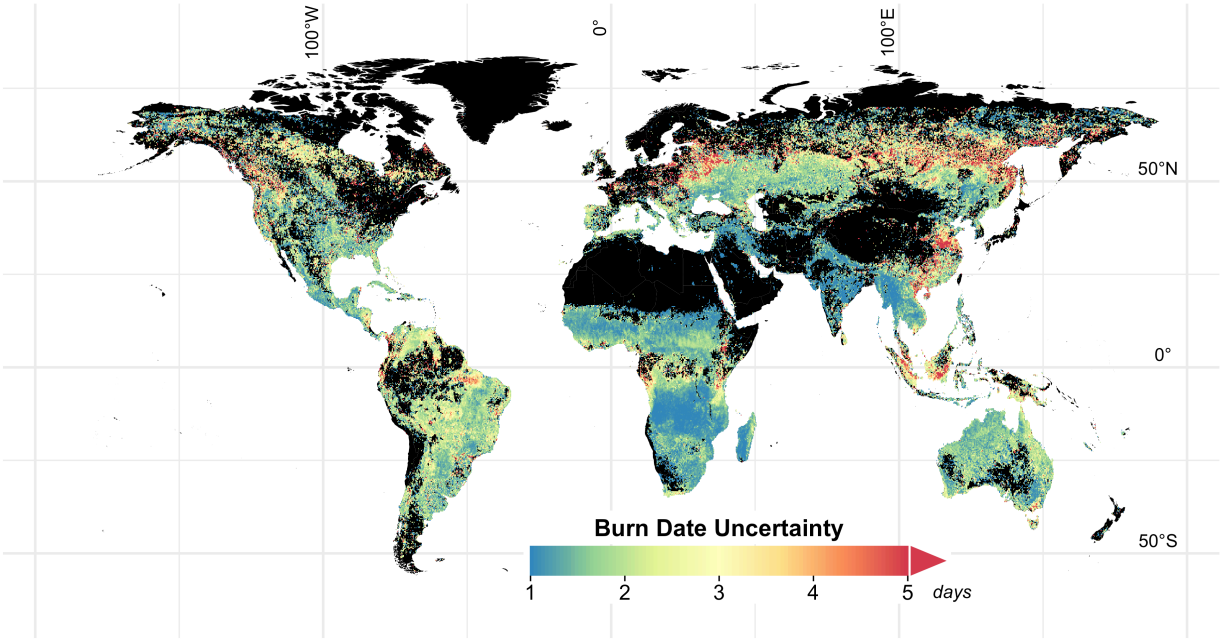

Figure S9. Average burn date uncertainty (in days), over 2003-2017, for burned area estimates from the MODIS MCD64A1 burned area product. The average burn date uncertainty is averaged over each grid cell at monthly timesteps and weighted by monthly burned area.

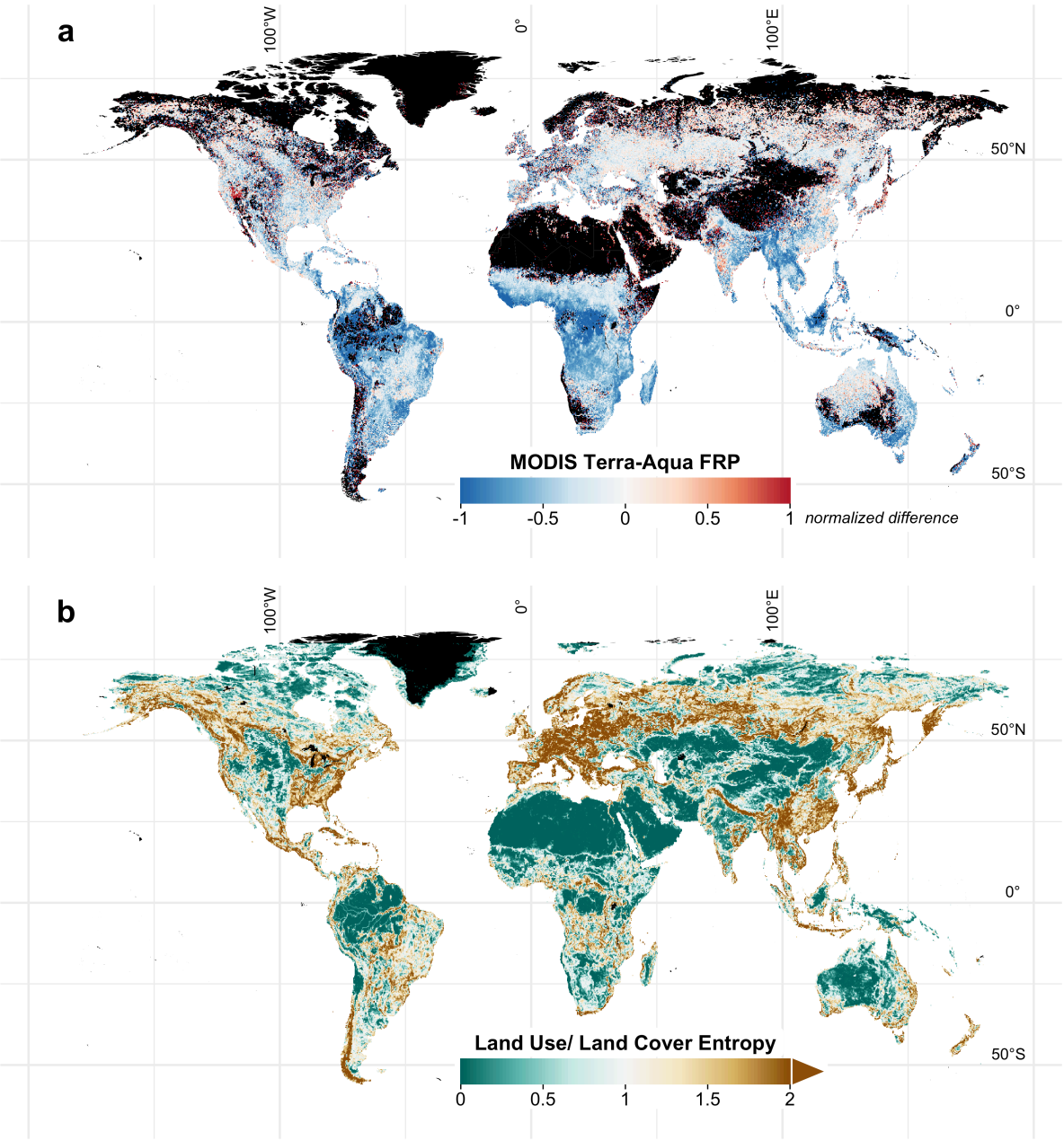

Figure S10. Ancillary information on the diurnal cycle in fire energy and entropy of land use/land cover classification, mapped at 0.25° x 0.25° spatial resolution. (**a**) MODIS FRP, from 2003-2017, expressed as the normalized difference of Terra and Aqua FRP. Positive values (red) indicate fire energy dominated by contribution from Terra (10:30 am overpass, morning), while negative values indicate fire energy dominated by contribution from Aqua (1:30 pm overpass, early afternoon). (**b**) Average entropy from MODIS MCD12Q1 Scheme 1 (IGBP) and Scheme 2 (UMD) land use/ land cover (LULC), from 2003-2016. We exclude pixels classified as water bodies or permanent snow/ice. Higher entropy (brown) indicates more heterogenous LULC; conversely, lower entropy (green) indicates more homogenous LULC.

S5. Fire Inventories: Regional Evaluation, Comparison, and Metrics (FIRECAM) online tool

We present an online tool called "Fire Inventories: Regional Evaluation, Comparison, and Metrics" (FIRECAM; https://globalfires.earthengine.app/view/firecam), hosted on Earth Engine Apps, that allows users to compare regional differences in five global fire emissions inventories (GFEDv4s, FINNv1.5, GFASv1.2, QFEDv2.5, and FEERv1.0-G1.2) for six species (CO_2, CO, CH_4, OC, BC, $PM_{2.5}$; Figure S11) and diagnose regional challenges in satellite observations of fires by using the five relative fire confidence metrics. We use the 14 "basis" regions defined in GFEDv4s as default, but users can also select a country, pixel, or custom region (Figure S12; van der Werf et al., 2017). Due to differences in spatial resolution, we aggregate all inventories to 0.5° x 0.5°.

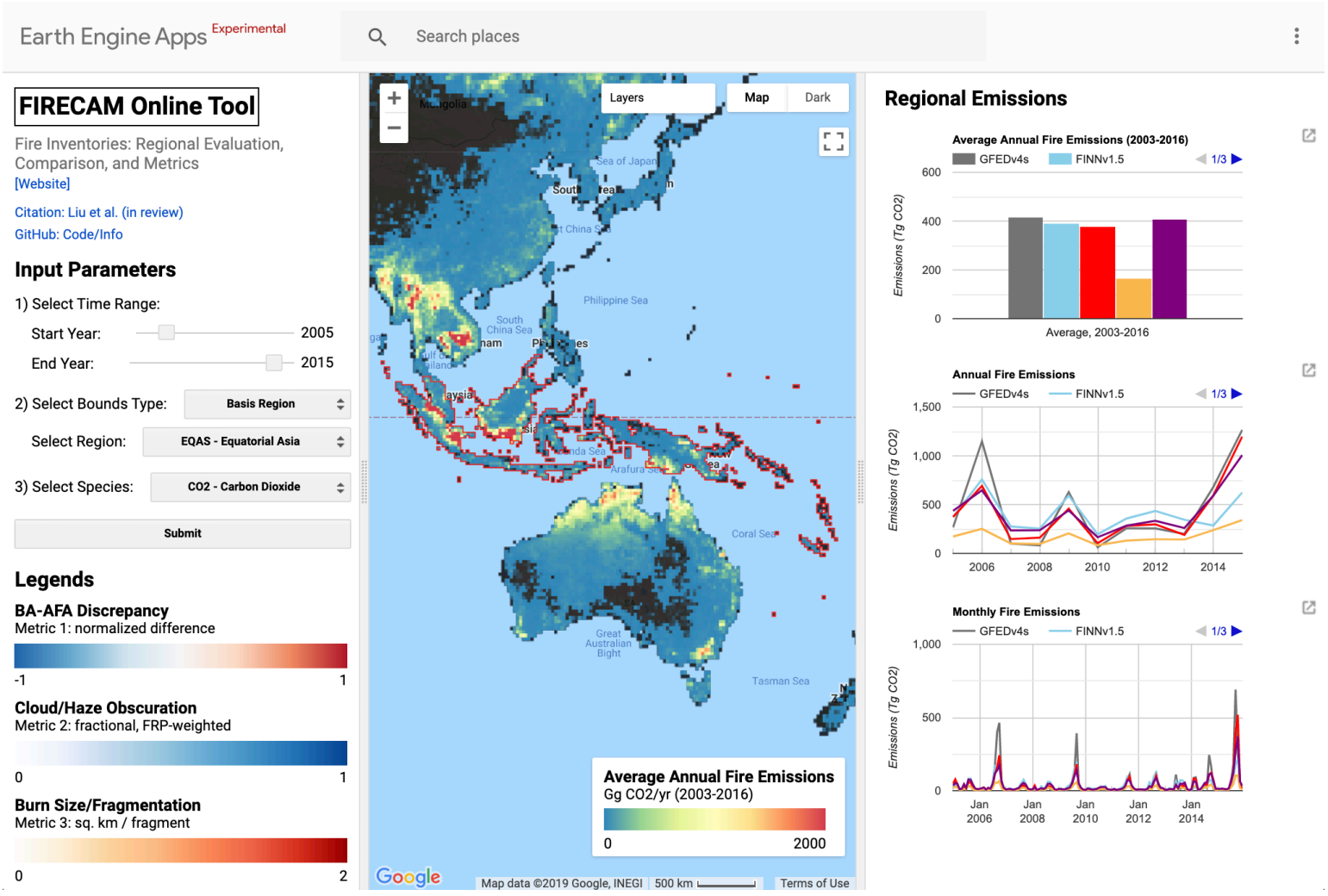

Figure S11. Screenshot of the Fire Inventories: Regional Evaluation, Comparison, and Metrics (FIRECAM) online tool (https://globalfires.earthengine.app/view/firecam).

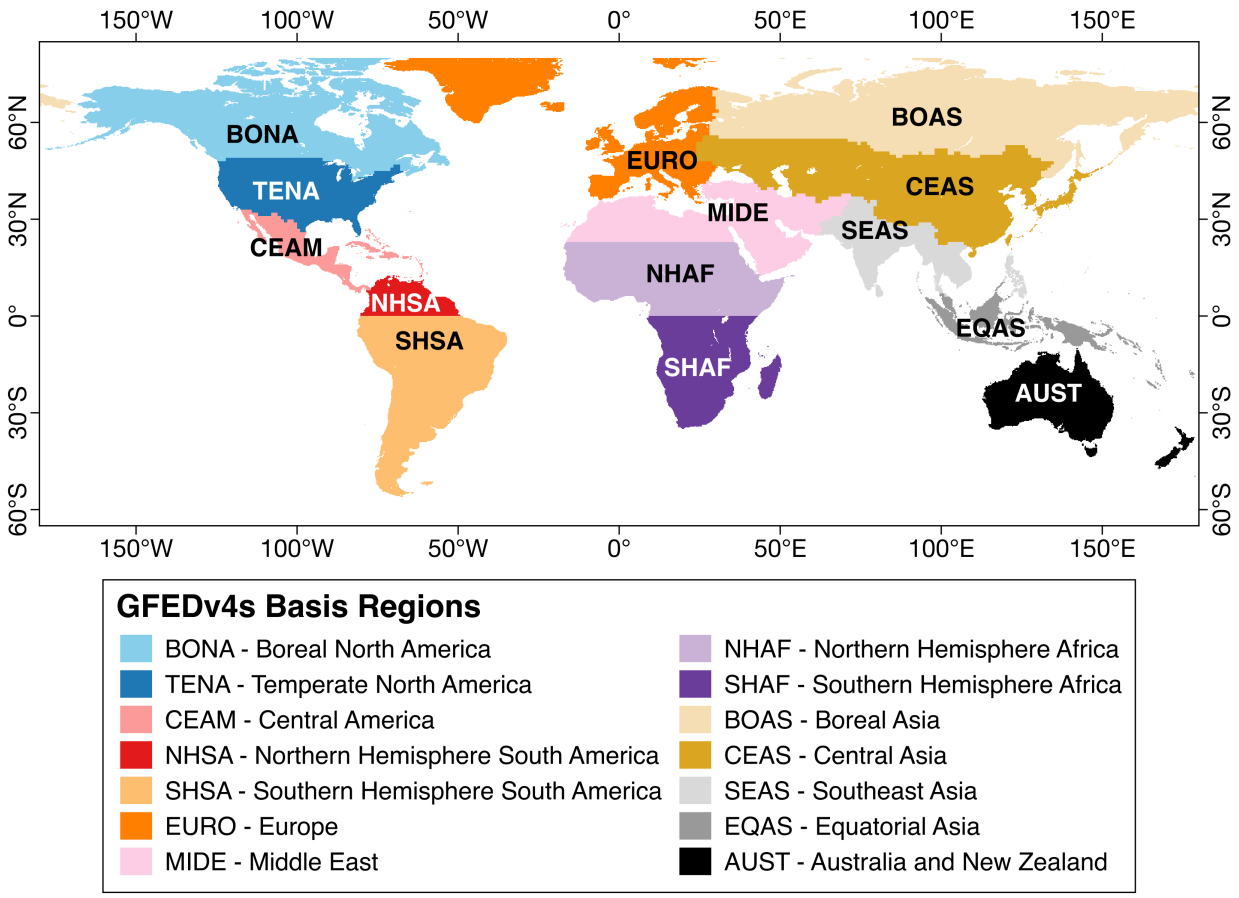

Figure S12. The 14 basis regions defined in GFEDv4s (van der Werf et al., 2017).

S6. Relative fire confidence metrics: consistency with other regional studies

The relative fire confidence metrics can be used to probe causes of region-specific uncertainties in satellite-observed fire activity. For example, how comparable are the challenges in estimating burned area in the agricultural region of eastern China compared to that in northern India? Given that eastern China has rougher terrain (metric 4) and much higher FRP-weighted cloud/haze fraction (metric 2) than India, we hypothesize that agricultural fire emissions in eastern China are more poorly constrained than those in India. We can further probe within-region differences in fire emissions estimates using the relative fire confidence metrics, as discussed below for wildland fires in the United States and for agricultural fires in India.

United States. Koplitz et al. (2018) compared wildland burned area and fire emissions from GFEDv4s, FINNv1.5, and the National Emission Inventory (NEI) from the U.S. Environmental Protection Agency (EPA). The NEI integrates satellite sources and on-the-ground reports and is considered most accurate of these inventories. These authors found that using FINNv1.5 and GFEDv4s in a regional model led to severe underestimates of 0.52-0.73 μg m^{-3} in the annual average $PM_{2.5}$ enhancement due to wildland fires over 2002-2014, relative to the NEI. However, compared to GFEDv4s, FINNv1.5 better captured the variability in burned area and pollutant concentrations in the U.S. Southeast. This last result is consistent with the high AFA-scores and low BA-scores over the U.S. Southeast, where small, fragmented fires dominate, as shown by metrics 1, 3, and 5 (McCarty et al., 2008). Given the moderate cloud/haze burden in this region (metric 2), top-down inventories that account for cloud gaps in the FRP record may be better suited for this region than bottom-up inventories.

India. During the post-monsoon season (Oct-Nov), smoke from agricultural fires in the northwestern states of Punjab and Haryana travels southeast across northern India, with severe consequences for air quality downwind. Small, fragmented fires dominate northwestern India (metrics 1, 3, and 5), leading to low BA-scores and high AFA-scores over the region; the flat topography (metric 4) and low cloud/haze fraction (metric 2) indicate that these two factors are not as important for evaluating satellite-derived fire activity in this region. High pFRP suggests that emissions from top-down inventories are uncertain, as many small fires may be missed. Using four different fire inventories (GFEDv4s, FINNv1.5, GFASv1.2, and QFEDv2.4), Cusworth et al. (2018) modeled smoke enhancement over Delhi during the 2012-2016 burning seasons. GFAS and GFEDv4s both strongly underestimated the smoke enhancement, compared to surface observations, while FINNv1.5 best captured this enhancement. Aside from the inherent difficulty of quantifying emissions from small agricultural fires, the strong afternoon peak in fire activity in northwestern India may also partially explain the GFEDv4s underestimate. This is because the small fires boost in GFED4s is derived from an average of Terra (morning) and Aqua (afternoon) estimates of active fires (Figure S10a; van der Werf et al., 2017). QFED leads to inconsistent smoke $PM_{2.5}$ enhancement over the 5 years, most notably yielding low enhancements in 2014 and 2016, when the influence of smoke on Delhi air quality appears to be greater. Both GFAS and QFED derive the conversion factor β of FRP to DM emissions based on earlier versions of GFED that do not apply a small fires boost, and this may explain the relatively low smoke $PM_{2.5}$ enhancement, at least for GFAS. QFED enhances aerosol emissions by a factor of 1.8 for savannas and grasslands, thus adjusting OC and BC emissions that might otherwise be too low.

S7. Trends in global fire emissions

The importance of inventory choice can further be seen in the estimated linear trends in global fire emissions. Trends in GFEDv4s and GFASv1.2 emissions, from 2003-2016, are statistically insignificant for most species while those in the other three inventories show statistically significant decreases (Table S3). While global burned area has declined over the past two decades (Andela et al., 2017), the trend in global fire emissions is not as clear due to the disproportionate contribution in emissions over burned area from some regions, such as Indonesia (van der Werf et al., 2017). The strong link between the El Niño Southern Oscillation and pan-tropical fires – Indonesian peat fires in particular – is responsible for emissions spikes in strong El Niño years, such as 2006 and 2015 (Chen et al., 2017; van der Werf et al., 2017). Peat delineation may be one factor that explain differences in trends using GFEDv4s and GFASv1.2 versus the three other inventories. However, further analysis is needed to determine the reasons for the presence or lack of statistically significant decreases in global fire emissions.

Evaluation of linear trends is an important application of global fire emissions inventories. As an example, Worden et al. (2017) pointed to linear trends in GFEDv4s emissions of CH_4 and to CO/CH_4 observations as evidence for the hypothesis that a decline in biomass burning over 2007-2014 can help explain isotopic changes in atmospheric methane after 2007. In fact, methane emissions from fires have not appreciably decreased according to GFEDv4s when this time period is extended to 2016. In any event, it is clear that inventory bias is an important factor to consider when drawing conclusions.

Table S3. Linear trends in global fire emissions, from 2003-2016, by inventory and species

	CO_2	**CO**	**CH_4**	**OC**	**BC**	**$PM_{2.5}$**
GFEDv4s	-68 (36)	-2.1 (2.6)	-0.03 (0.2)	-0.09 (0.12)	-0.02 (0.01)	-0.27 (0.21)
FINNv1.5	**-180 (48)**	**-9.3 (2.6)**	**-0.43 (0.13)**	**-0.57 (0.16)**	**-0.05 (0.01)**	**-1.0 (0.28)**
GFASv1.2	-71 (36)	-3 (2.8)	-0.12 (0.24)	-0.15 (0.14)	**-0.03 (0.01)**	-0.32 (0.21)
QFEDv2.5r1	**-113 (32)**	**-5.5 (1.4)**	**-0.26 (0.06)**	**-0.74 (0.24)**	**-0.08 (0.02)**	**-1.17 (0.36)**
FEERv1.0-G1.2	**-169 (53)**	**-8.3 (2.6)**	**-0.43 (0.14)**	**-0.4 (0.14)**	**-0.05 (0.02)**	**-0.69 (0.23)**

Statistically significant trends ($p < 0.05$) are bolded. Standard error is in parentheses.

S8. Implementation of global fire emissions inventories in GEOS-Chem

As an example of how the emissions implemented into chemical transport models (CTMs) may be outdated, we examine the implementation of GFED, FINN, and QFED into GEOS-Chem. The GEOS-Chem CTM (geos-chem.org) is paired with the Harvard-NASA Emissions Component (HEMCO; Keller et al., 2014), an interface for emissions inventories. The default global fire emissions inventory in GEOS-Chem CTM is GFED, with an option to use QFED or FINN. The current versions of GFED, FINN, and QFED available in HEMCO are GFEDv4s, FINNv1.5, and QFEDv2.5.

First, as new versions of emissions inventories become available, such updates may lag months to years before full incorporation into GEOS-Chem. For example, GFEDv4s updated emissions factors in 2017 (van der Werf et al., 2017), but this change was made available only in March 2018 and fully implemented in GEOS-Chem v12 in August 2018. Using updated emissions factors decreases average annual global emissions, from 2003-2016, of CH_4, OC, and BC by 8.6-13%, and the other emissions by lesser amounts (Table S4). In particular, the BC emissions factor for peatlands decreased by 93% from 0.566 to 0.04 g BC/kg DM with updated emissions factors (van der Werf et al., 2017; Table S5). This is more consistent with measurements that suggest the peat BC emissions factor is almost negligible due to the lack of flaming fires in peatlands (Stockwell et al., 2016). Further, QFED was updated to v2.5r1 in HEMCO in July 2018 with no intermediate versions (e.g., v2.4r8) superseding v2.4r6 since September 2014. QFEDv2.5r1, which reflects the update in MODIS active fires from C5 to C6, has been available from the NASA Center for Climate Simulation (NCCS) data portal (https://portal.nccs.nasa.gov/datashare/iesa/aerosol/emissions/QFED/v2.5r1/) since December 2016, and QFEDv2.4r8 since April 2015.

Second, we find inconsistencies between emissions from the "out-of-box" FINNv1.5, downloaded from http://bai.acom.ucar.edu/Data/fire/, and FINNv1.5 in HEMCO. FINNv1.5 in HEMCO is gridded to 0.25° x 0.25° for CO_2 only. Scaling factors are then used to convert CO_2 to other species. This approach, which is also used with GFED dry matter (DM) emissions, conserves storage and limits computational cost. We separately calculate the average yearly emissions from 2003-2016 for CO_2, CO, CH_4, OC, and BC for "out-of-box" and HEMCO versions. While CO_2, CO, CH_4 emissions differ by < 1%, OC emissions are 14% lower in HEMCO than in FINNv1.5, and BC emissions 36% higher (Table S6). Discrepancies are present for all scaling factors, but appreciable differences in CO_2/OC and CO_2/BC for class 2, or woody savanna, are primarily responsible for the large relative error in OC and BC emissions (Table S7). Additionally, FINNv1.5 in HEMCO is missing class 6, or temperate evergreen forest. For classes 3-5, we find two unique scaling factors each for "out-of-box" FINNv1.5. These discrepancies imply that FINNv1.5 must be implemented with all species independently calculated, similar to QFED in HEMCO, or that FINNv1.5 LULC should be further subdivided to account for the unique scaling factors.

In summary, emissions inventories may lag in version as implemented in CTMs, as in the case of QFED in GEOS-Chem. Our results imply non-negligible impacts on the emissions budget from (1) outdated emissions factors for GFEDv4s and (2) errors in the implementation of

FINNv1.5 in GEOS-Chem, with implications for studies that used these inventories in GEOS-Chem.

Table S4. Differences in mean annual global GFEDv4s CO_2, CO, CH_4, OC, and BC emissions (Tg yr^{-1}, ±1σ) using the original and updated emissions factors.

	CO_2	**CO**	**CH_4**	**OC**	**BC**
Old EFs, *pre-GCv12* (Tg)	6825 (584)	331 (40)	17 (3)	17 (2)	2.1 (0.2)
New EFs, *GCv12* (Tg)	6986 (595)	336 (39)	15 (3)	16 (2)	1.8 (0.2)
Relative Diff. (%)	2.4	1.5	-13	-8.6	-13

Table S5. Differences in original and updated emissions factors (EFs; g species kg^{-1} dry matter) for GFEDv4s. The original EFs were available with the July 2015 release of GFEDv4s and updated in June 2017 in van der Werf et al. (2017).

		CO_2	**CO**	**CH_4**	**OC**	**BC**
Class 1: SAVA *Savannas, grasslands, shrublands*	Original EFs	1650	62.3	2.2	3.21	0.46
	Updated EFs	1686	63	1.94	2.62	0.37
Class 2: BORF *Boreal forests*	Original EFs	1570	106	4.81	9.15	0.562
	Updated EFs	1489	127	5.96	9.6	0.5
Class 3: TEMF *Temperate forests*	Original EFs	1570	106	4.81	9.15	0.562
	Updated EFs	1647	88	3.36	9.6	0.5
Class 4: DEFO *Tropical forests and deforestation*	Original EFs	1630	101	6.59	4.3	0.566
	Updated EFs	1643	93	5.07	2.71	0.52
Class 5: PEAT *Peatlands*	Original EFs	1710	210	20.8	4.3	0.566
	Updated EFs	1703	210	20.8	6.02	0.04
Class 6: AGRI *Agricultural*	Original EFs	1310	92.1	8.79	4.14	0.42
	Updated EFs	1585	102	8.4	2.3	0.75

Table S6. Differences in mean annual global CO_2, CO, CH_4, OC, and BC emissions (Tg yr^{-1}, ±1σ) between "out-of-box" and HEMCO FINNv1.5

	CO_2	**CO**	**CH_4**	**OC**	**BC**
Out-of-box (Tg)	6292 (1137)	330 (60)	16 (3)	20 (4)	1.9 (0.3)
HEMCO (Tg)	6309 (1019)	330 (53)	16 (3)	17 (3)	2.6 (0.4)
Relative Error (%)	0.3	-0.2	0.3	-14	36

Table S7. Differences in scaling factors from CO_2 to CO, CH_4, OC, and BC emissions between "out-of-box" and HEMCO FINNv1.5

		CO_2/CO (mole/mole)	**CO_2/CH_4** (mole/mole)	**CO_2/OC** (mole/g)	**CO_2/BC** (mole/g)
Class 1 *Savanna, grasslands*	Out-of-box	18.3	411.1	14.8	103.9
	HEMCO	17	316.7	14.7	103.5
Class 2 *Woody savanna*	Out-of-box	16.1	240.5	5.9	78
	HEMCO	15.3	226.5	10.5	29.8
Class 3 *Tropical forest*	Out-of-box	7.9, 11.4	98.1, 117.4	4.5, 7.9	61.3, 71.8
	HEMCO	11.2	118.1	7.9	71.8
Class 4 *Temperate forest*	Out-of-box	7.5, 7.9	90.4, 98.1	4.3, 4.5	61.3, 169.2
	HEMCO	10.3	127.7	4	65.1
Class 5 *Boreal forest*	Out-of-box	7.5, 7.9	90.4, 98.1	4.3, 4.5	61.3, 169.2
	HEMCO	7.5	91.1	4.3	169.2
Class 6 *Temperate evergreen forest*	Out-of-box	11.9	178.7	4.9	66.8
	HEMCO	x	x	x	x
Class 9 *Agricultural*	Out-of-box	8.8	93.4	10.6	50.6
	HEMCO	9.9	99.3	15.7	48

References

Andela, N., Morton, D.C., Giglio, L., Chen, Y., van der Werf, G.R., Kasibhatla, P.S., DeFries, R.S., Collatz, G.J., Hantson, S., Kloster, S., Bachelet, D., Forrest, M., Lasslop, G., Li, F., Mangeon, S., Melton, J.R., Yue, C., Randerson, J.T., 2017. A human-driven decline in global burned area. Science. 356, 1356–1362. https://doi.org/10.1126/science.aal4108

Chen, Y., Morton, D.C., Andela, N., van der Werf, G.R., Giglio, L., Randerson, J.T., 2017. A pan-tropical cascade of fire driven by El Niño/Southern Oscillation. Nat. Clim. Chang. 7, 906–911. https://doi.org/10.1038/s41558-017-0014-8

Christian, T.J., Kleiss, B., Yokelson, R.J., Holzinger, R., Crutzen, P.J., Hao, W.M., Saharjo, B.H., Ward, D.E., 2003. Comprehensive laboratory measurements of biomass-burning emissions: 1. Emissions from Indonesian, African, and other fuels. J. Geophys. Res. 108, 4719. https://doi.org/10.1029/2003JD003704

CIESIN, 2017. Gridded Population of the World, Version 4 (GPWv4): Population Count Adjusted to Match 2015 Revision of UN WPP Country Totals, Revision 10.

Darmenov, A.S., da Silva, A., 2013. The Quick Fire Emissions Dataset (QFED) - Documentation of versions 2.1, 2.2, and 2.4, NASA Technical Report Series on Global Modeling and Data Assimilation, Volume 32.

Di Giuseppe, F., Rémy, S., Pappenberger, F., Wetterhall, F., 2017. Improving forecasts of biomass burning emissions with the fire weather index. J. Appl. Meteorol. Climatol. 56, 2789–2799. https://doi.org/10.1175/JAMC-D-16-0405.1

Giglio, L., Randerson, J.T., van der Werf, G.R., 2013. Analysis of daily, monthly, and annual burned area using the fourth-generation global fire emissions database (GFED4). J. Geophys. Res. Biogeosciences 118, 1–12. https://doi.org/10.1002/jgrg.20042

Giglio, L., Schroeder, W., Justice, C.O., 2016. The collection 6 MODIS active fire detection algorithm and fire products. Remote Sens. Environ. 178, 31–41. https://doi.org/10.1016/j.rse.2016.02.054

Heil, A., Kaiser, J.W., van der Werf, G.R., Wooster, M.J., Schultz, M.G., van der Gon, H.D., 2010. Assessment of the Real-Time Fire Emissions (GFASv0) by MACC, ECMWF Techical Memo No. 626.

Ichoku, C., Ellison, L., 2014. Global top-down smoke-aerosol emissions estimation using satellite fire radiative power measurements. Atmos. Chem. Phys. 14, 6643–6667. https://doi.org/10.5194/acp-14-6643-2014

Kaiser, J.W., Heil, A., Andreae, M.O., Benedetti, A., Chubarova, N., Jones, L., Morcrette, J.J., Razinger, M., Schultz, M.G., Suttie, M., van der Werf, G.R., 2012. Biomass burning emissions estimated with a global fire assimilation system based on observed fire radiative power. Biogeosciences 9, 527–554. https://doi.org/10.5194/bg-9-527-2012

Keller, C.A., Long, M.S., Yantosca, R.M., Da Silva, A.M., Pawson, S., Jacob, D.J., 2014. HEMCO v1.0: A versatile, ESMF-compliant component for calculating emissions in atmospheric models. Geosci. Model Dev. 7, 1409–1417. https://doi.org/10.5194/gmd-7-1409-2014

Khan, M.F., Latif, M.T., Juneng, L., Amil, N., Nadzir, M.S.M., Hoque, H.M.S., 2015. Physicochemical factors and sources of particulate matter at residential urban environment in Kuala Lumpur. J. Air Waste Manag. Assoc. 65, 958–969. https://doi.org/10.1080/10962247.2015.1042094

Kuwata, M., Neelam-Naganathan, G.-G.G., Miyakawa, T., Khan, M.F., Kozan, O., Kawasaki, M., Sumin, S., Latif, M.T., 2018. Constraining the Emission of Particulate Matter From Indonesian Peatland Burning Using Continuous Observation Data. J. Geophys. Res. Atmos. 123, 9828–9842. https://doi.org/10.1029/2018JD028564

McCarty, J.L., Loboda, T., Trigg, S., 2008. A hybrid remote sensing approach to quantifying crop residue burning in the United States. Appl. Eng. Agric. 24, 515–527. https://doi.org/10.13031/2013.25137

Mu, M., Randerson, J.T., Van Der Werf, G.R., Giglio, L., Kasibhatla, P., Morton, D., Collatz, G.J., Defries, R.S., Hyer, E.J., Prins, E.M., Griffith, D.W.T., Wunch, D., Toon, G.C., Sherlock, V., Wennberg, P.O., 2011. Daily and 3-hourly variability in global fire emissions and consequences for atmospheric model predictions of carbon monoxide. J. Geophys. Res. Atmos. 116, D24303. https://doi.org/10.1029/2011JD016245

Olson, D.M., Dinerstein, E., Wikramanayake, E.D., Burgess, N.D., Powell, G.V.N., Underwood, E.C., D'amico, J.A., Itoua, I., Strand, H.E., Morrison, J.C., Loucks, C.J., Allnutt, T.F., Ricketts, T.H., Kura, Y., Lamoreux, J.F., Wettengel, W.W., Hedao, P., Kassem, K.R., 2001. Terrestrial Ecoregions of the World: A New Map of Life on Earth. Bioscience 51, 933. https://doi.org/10.1641/0006-3568(2001)051[0933:TEOTWA]2.0.CO;2

Randerson, J.T., Chen, Y., van der Werf, G.R., Rogers, B.M., Morton, D.C., 2012. Global burned area and biomass burning emissions from small fires. J. Geophys. Res. Biogeosciences 117, G04012. https://doi.org/10.1029/2012JG002128

Stockwell, C.E., Jayarathne, T., Cochrane, M.A., Ryan, K.C., Putra, E.I., Saharjo, B.H., Nurhayati, A.D., Albar, I., Blake, D.R., Simpson, I.J., Stone, E.A., Yokelson, R.J., 2016. Field measurements of trace gases and aerosols emitted by peat fires in Central Kalimantan, Indonesia, during the 2015 El Niño. Atmos. Chem. Phys. 16, 11711–11732. https://doi.org/10.5194/acp-16-11711-2016

van der Werf, G.R., Randerson, J.T., Giglio, L., Collatz, G.J., Mu, M., Kasibhatla, P.S., Morton, D.C., Defries, R.S., Jin, Y., Van Leeuwen, T.T., 2010. Global fire emissions and the contribution of deforestation, savanna, forest, agricultural, and peat fires (1997-2009). Atmos. Chem. Phys. 10, 11707–11735. https://doi.org/10.5194/acp-10-11707-2010

van der Werf, G.R., Randerson, J.T., Giglio, L., van Leeuwen, T.T., Chen, Y., Rogers, B.M., Mu, M., van Marle, M.J.E., Morton, D.C., Collatz, G.J., Yokelson, R.J., Kasibhatla, P.S., 2017. Global fire emissions estimates during 1997–2016. Earth Syst. Sci. Data 9, 697–720. https://doi.org/10.5194/essd-9-697-2017

Wiedinmyer, C., Akagi, S.K., Yokelson, R.J., Emmons, L.K., Orlando, J.J., Soja, A.J., 2011. The Fire INventory from NCAR (FINN): a high resolution global model to estimate the emissions from open burning. Geosci. Model Dev. 4, 625–641. https://doi.org/10.5194/gmd-4-625-2011

Worden, J.R., Bloom, A.A., Pandey, S., Jiang, Z., Worden, H.M., Walker, T.W., Houweling, S.,

Röckmann, T., 2017. Reduced biomass burning emissions reconcile conflicting estimates of the post-2006 atmospheric methane budget. Nat. Commun. 8, 2227. https://doi.org/10.1038/s41467-017-02246-0